Hydrogen Transfer between Sulfuric Acid and Hydroxyl Radical in the Gas Phase: Competition among Hydrogen Atom Transfer, Proton-Coupled Electron-Transfer, and Double Proton Transfer

Josep M. Anglada,*,† Santiago Olivella,*,† and Albert Solé‡

Institut d'Investigacions Químiques i Ambientals de Barcelona, CSIC, Jordi Girona 18, 08034-Barcelona, Catalonia, Spain, and Centre Especial de Recerca en Química Teòrica i Departament de Química Física, Universitat de Barcelona, Martí i Franquès 1, 08028-Barcelona, Catalonia, Spain

Received: October 26, 2005; In Final Form: November 28, 2005

In an attempt to assess the potential role of the hydroxyl radical in the atmospheric degradation of sulfuric acid, the hydrogen transfer between H_2SO_4 and $HO^\bullet$ in the gas phase has been investigated by means of DFT and quantum-mechanical electronic-structure calculations, as well as classical transition state theory computations. The first step of the $H_2SO_4 + HO^\bullet$ reaction is the barrierless formation of a prereactive hydrogen-bonded complex (**Cr1**) lying 8.1 kcal mol^{-1} below the sum of the (298 K) enthalpies of the reactants. After forming **Cr1**, a single hydrogen transfer from H_2SO_4 to $HO^\bullet$ and a degenerate double hydrogen-exchange between H_2SO_4 and $HO^\bullet$ may occur. The single hydrogen transfer, yielding $HSO_4^\bullet$ and H_2O, can take place through three different transition structures, the two lowest energy ones (**TS1** and **TS2**) corresponding to a proton-coupled electron-transfer mechanism, whereas the higher energy one (**TS3**) is associated with a hydrogen atom transfer mechanism. The double hydrogen-exchange, affording products identical to reactants, takes place through a transition structure (**TS4**) involving a double proton-transfer mechanism and is predicted to be the dominant pathway. A rate constant of 1.50×10^{-14} cm^3 $molecule^{-1}$ s^{-1} at 298 K is obtained for the overall reaction $H_2SO_4 + HO^\bullet$. The single hydrogen transfer through **TS1**, **TS2**, and **TS3** contributes to the overall rate constant at 298 K with a 43.4%. It is concluded that the single hydrogen transfer from H_2SO_4 to $HO^\bullet$ yielding $HSO_4^\bullet$ and H_2O might well be a significant sink for gaseous sulfuric acid in the atmosphere.

1. Introduction

Sulfuric acid (H_2SO_4) plays an important role in the chemistry of the atmosphere. It contributes to the acid rain on the Earth's surface. The acid rain is spread out through surface waters, can have a pH as low as 4 in certain areas, and produces extensive ecological damage.[1−3] Moreover, H_2SO_4 is also related to the formation of sulfate aerosols, affecting clouds, precipitation, and radiation balance, and, therefore, having a direct influence in the climate change.[4−7] H_2SO_4 is formed in the troposphere by oxidation of SO_2, which is emitted to the atmosphere in amounts close to 100 Tg yr^{-1}.[8,9] The oxidation of SO_2 takes place either in clouds (about 90%) by oxidants like O_3 and H_2O_2 or in gas phase (about 10%),[1,8] in a process that is believed to occur by a series of three reactions as follows:

$$SO_2 + HO^\bullet + M \rightarrow HOSO_2^\bullet + M \quad (1)$$

$$HOSO_2^\bullet + O_2 \rightarrow SO_3 + HO_2^\bullet \quad (2)$$

$$SO_3 + H_2O + M \rightarrow H_2SO_4 + M \quad (3)$$

where M stands for a collision partner. Reaction eq 3 seems to require the concurrence of several water molecules.[10−17]

Once formed, gaseous H_2SO_4 has so little vapor pressure at the temperature ranges of atmospheric interest (below 3.0×10^{-5} Torr) that is commonly assumed to condense out onto aerosol particle surfaces. Current measurements of gaseous H_2SO_4 levels in the troposphere showed a rather low concentration with values ranging from 1.6×10^5 to 9.0×10^7 molecules cm^{-3}.[18,19] Although dry deposition (sulfate aerosols) and wet precipitation (acid rain) are undoubtedly the main process for physical removal of H_2SO_4 from the atmosphere, we though it could be interesting to explore possible atmospheric chemical reactions of gaseous H_2SO_4 leading to its degradation. Since the reaction of the hydroxyl radical ($HO^\bullet$) with nitric acid (HNO_3) and formic acid (HCOOH) plays a significant role in the atmospheric fate of these acids,[2,20−25] it is likely that the reaction of $HO^\bullet$ with H_2SO_4 can also contribute to the atmospheric degradation of the latter acid. In general, $HO^\bullet$ reacts with nonradical atmospheric species by abstracting hydrogen atoms. Thus, in the case of H_2SO_4, the following hydrogen atom abstraction reaction can be envisaged

$$H_2SO_4 + HO^\bullet \rightarrow HSO_4^\bullet + H_2O \quad (4)$$

The aim of this theoretical study is to determine whether H_2SO_4 reacts with $HO^\bullet$ in the gas phase and to assess the potential role of this reaction in the atmospheric degradation of gaseous H_2SO_4. In this study, we focus on the mechanisms of the hydrogen transfer between the reactants. To this end, density functional theory (DFT) and ab initio quantum-mechanical electronic structure calculations were carried out on the ground-state potential energy surface (PES) of the $H_2SO_4 + HO^\bullet$ reaction system in the gas phase. In addition, an estimation of the rate constants of the different elementary reactions consid-

* Corresponding authors. E-mail: jarqtc@cid.csic.es and sonqtc@cid.csic.es.
† Institut d'Investigacions Químiques i Ambientals de Barcelona, CSIC.
‡ Centre Especial de Recerca en Química Teòrica and Departament de Química Física, Universitat de Barcelona.

10.1021/jp056155g CCC: $33.50
Published on Web 12/24/2005

ered was performed by using classical transition state theory. To our knowledge, this is the first theoretical study of the $H_2SO_4 + HO^{\bullet}$ reaction.

2. Computational Details

All stationary points on the ground-state PES of the $H_2SO_4 + HO^{\bullet}$ reaction system were fully optimized using the spin-unrestricted version of the Becke three-parameter hybrid functional[26] combined with the Lee, Yang, and Parr correlation functional,[27] denoted as UB3LYP,[28] with the split-valence 6-311+G(2df,2p) basis set,[29] which includes a single diffuse sp shell on carbon, oxygen, and sulfur atoms,[30] double d-polarization and a single additional f-polarization on carbon, oxygen, and sulfur atoms and double p-polarization on hydrogen atoms. At this level of theory the harmonic vibrational frequencies were also calculated to verify the nature of the corresponding stationary point (minimum or transition structure) and to provide the zero-point vibrational energy (ZPVE), the thermal correction to enthalpy, absolute entropy, and Gibbs free energy, assuming ideal gas behavior and a standard pressure of 1 atm. Moreover, to ensure that the transition structures connect the desired reactants and products, intrinsic reaction coordinate (IRC)[31,32] calculations[33,34] were performed at the UB3LYP/6-311+G(2df,2p) level of theory for each transition structure.

To assess the reliability of the UB3LYP calculations, the geometries and harmonic vibrational frequencies of the transition structures found at this level of theory were also calculated by using (frozen core) quadratic configuration interaction with the singles and doubles method, based on the spin-unrestricted Hartree−Fock (UHF) method reference determinant,[35] designated as UQCISD, in conjunction to the split-valence 6-31+G-(d,p) basis set.[29]

Since it is well-known that the UB3LYP functional underestimates the energy barriers calculated for free radical H atom abstraction reactions,[36] we carried out single-point (frozen core) coupled-cluster[37] calculations including all single and double excitations, based on a reference UHF single determinant, together with a perturbative treatment of all connected triple excitations,[38] denoted as UCCSD(T), using the geometries optimized at the UB3LYP/6-311+G(2df,2p) level. Dunning's correlation-consistent polarized valence triple-ζ (cc-pVTZ) basis set[39,40] was employed in the UCCSD(T) calculations. Moreover, for the different hydrogen-bonded complexes found in this work, the basis set superposition error (BSSE) was calculated at the UCCSD(T)/cc-pVTZ level by using the counterpoise method of Boys and Bernardi.[41] The bonding features of the different stationary points were examined by performing an analysis of the electron charge and electron spin density within the framework of the topological theory of atoms in molecules (AIM). The first-order density matrix obtained from UB3LYP calculations with the 6-311+G(2df,2p) basis set was used in this analysis. The theory of AIM has been reviewed in the literature and in a monograph.[42] For the convenience of the reader, we will summarize some important points here. The topological characteristics of the electronic charge density $\rho(\mathbf{r})$ ($\mathbf{r} \in x, y, z$) give rise to a rigorous partitioning of the real space comprising a molecule into different atomic basins. In AIM theory, an atom consists of a nucleus and its associated atomic basin. Properties like charges, dipole, and quadrupole moments can thus unequivocally be assigned to individual atoms by integration of the desired property over their atomic basin. Chemical bonds between pairs of atoms can be identified by (3,−1) critical points (also called "bond critical points") of the electronic charge density $\rho(\mathbf{r})$. At such points $\mathbf{r}_b$ the gradient vector of $\rho(\mathbf{r})$ vanishes. The notation (3,−1) implies that, in addition, the Hessian matrix of $\rho(\mathbf{r})$ at $\mathbf{r}_b$ has three nonvanishing eigenvalues, two of which are negative and one positive. The line of maximum charge density linking the nuclei of the pairs of atoms passes through $\mathbf{r}_b$. This line is called a bond path. The charge density at the bond critical point, $\rho(\mathbf{r}_b)$, provides a measure for the covalent bond order between a given pair of atoms. Furthermore, the value of the Laplacian of $\rho(\mathbf{r})$ at the bond critical point, $\nabla^2\rho(\mathbf{r}_b)$, i.e., the sum of the three eigenvalues of Hessian matrix, indicates whether covalent or closed-shell interaction prevail between the two bonded atoms. $\nabla^2\rho(\mathbf{r})$ identifies regions of space wherein $\rho(\mathbf{r})$ is locally concentrated ($\nabla^2\rho(\mathbf{r}) < 0$) or depleted ($\nabla^2\rho(\mathbf{r}) > 0$). Therefore, a negative value of $\nabla^2\rho(\mathbf{r})$ in the internuclear region of two interacting atoms implies the formation of a covalent bond, since electron density is built up in that region, while positive values indicate are characteristic of closed-shell interactions, such as ionic, van der Waals, and hydrogen bonding, where the electron density is depleted from the internuclear region and concentrated on the corresponding atomic basins. Useful information is also related to (3,+1) critical points of the electron density (also called "ring critical points"). The notation (3,+1) implies that the Hessian matrix of $\rho(\mathbf{r})$ at such points $\mathbf{r}_r$ has three nonvanishing eigenvalues, two of which are positive. A ring critical point occurs as consequence of the fact that some bond paths are linked so as to form a ring of bonded atoms. Then a ring critical point is found in the interior of the ring.

Finally, the rate constants for the elementary reactions considered were calculated by using classical transition state theory. The UCCSD(T)/cc-pVTZ energies and the UB3LYP/6-311+G(2df,2p) partition functions were employed in these calculations. The tunneling corrections to the rate constants were computed by the zero order approximation to the vibrationally adiabatic PES with zero curvature. In this case, the potential energy curve was approximated by using an unsymmetrical Eckart potential energy barrier.[43]

All UB3LYP, UQCISD, and UCCSD(T) calculations were carried out with GAUSSIAN 98 program package.[44] The electronic features of the different stationary points were visualized with the Molden program[45] and the topological analysis of the electron charge and spin density calculations made use of a locally modified version[46] of the PROAIM and EXTREME programs of Bader et al.[47,48] The kinetic results were obtained with the TheRate program.[49]

3. Electronic Structure Considerations

Recently, it has been pointed out that the hydrogen transfer from the OH group to oxygen-centered radicals in the gas phase can occur in different ways.[50−52] In the particular case of the hydrogen transfer reaction (eq 4), the relative orientation of the hydroxyl radical approaching sulfuric acid leads to three different reaction modes with distinct electronic structure features, which are pictorially represented in Scheme 1.

In the first reaction mode (Scheme 1a) the hydroxyl radical is oriented in such a way that its unpaired electron interacts with a hydrogen atom of the sulfuric acid, giving a three-center three-electron bond in the transition state, in which the unpaired electron of the hydroxyl radical is delocalized over the oxygen atoms that undergo hydrogen exchange. This pathway leads to a simple hydrogen atom transfer from the acid to the hydroxyl radical. In other words, the reaction takes place via a *hydrogen atom transfer* (HAT) mechanism in which the proton and the electron are transferred together as a hydrogen atom. HAT is the conventional radical hydrogen atom abstraction mechanism of organic free-radical chemistry.

SCHEME 1: Pictorial Representation of the Electronic Structure Features of Three Different Reaction Modes for Hydrogen Transfer between H_2SO_4 and HO•

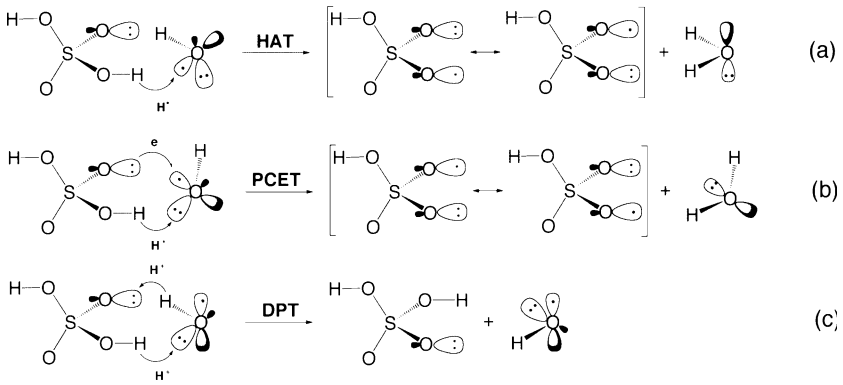

In the second reaction mode (Scheme 1b) the hydroxyl radical lone pair of electrons is directed toward a hydrogen atom of the sulfuric acid, while its unpaired electron interacts with the lone pair of electrons of an oxygen atom of the sulfuric acid. This approach of the reactants involves a S−OH···: OH hydrogen bond and a S═O: ····OH two-center three-electron interaction leading to the transfer of one electron from S═O: to HO• coupled with a transfer of a proton from the S−OH to HO•. That is, the reaction takes place v*ia a proton-coupled electron-transfer* (PCET) mechanism.[53] The net result of this process is identical to that of the HAT mechanism, namely the transfer of a hydrogen atom from the sulfuric acid to the hydroxyl radical (eq 4). As pointed out in ref 51, the PCET mechanism intends to avoid the so-called triplet repulsion[54−58] between the oxygen atoms that undergo hydrogen exchange in the HAT transition state, $[O^{\uparrow}\cdots H^{\downarrow}\cdots O^{\uparrow}]^{\ddagger}$, caused by the necessary occurrence of parallel electron spin on these atoms during the course of the reaction.

Finally, in the third reaction mode (Scheme 1c) the unpaired electron of the hydroxyl radical remains in a 2p orbital of the oxygen atom perpendicular to the O═S−OH plane during the course of the reaction and the lone pair of electrons of the hydroxyl radical is directed toward a hydrogen atom of the sulfuric acid, while the hydrogen atom of the hydroxyl radical interacts with the lone pair of electrons of an oxygen atom of the sulfuric acid. The S−OH···: OH and S═O: ···HO• interactions arising in this reaction mode lead to a *double proton transfer* (DPT) mechanism, namely the transfer of a proton from the sulfuric acid to the hydroxyl radical with the simultaneous transfer of a proton from the hydroxyl radical to an oxygen atom of the sulfuric acid. Consequently, in this reaction (eq 5) the reactants and products are the same species, so it is a degenerate double hydrogen-exchange reaction.

$$H_2SO_4 + HO^{\bullet} \rightarrow H_2SO_4 + HO^{\bullet} \qquad (5)$$

4. Results and Discussion

The calculations carried out in the present work indicate the existence of four elementary pathways for the gas-phase reaction between H_2SO_4 and HO• involving hydrogen transfer between these reactants. Figures 1 and 2 show the most relevant geometrical parameters of all the stationary points found on these pathways at the UB3LYP/6-311+G(2df,2p)[59] level and Figure 3 displays schematically the corresponding energy profiles, along with the atom numbering of each stationary point. Total electronic energies, ZPVEs, enthalpies, Gibbs free-energies, and absolute entropies are collected in Table 2S (Supporting Information). Table 1 gives the relative energies (ΔU), the relative energies at 0 K (ΔE(0 K)), the relative enthalpies at 298 K (ΔH(298 K)), and the Gibbs free energies at 298 K (ΔG(298 K)), calculated at the UCCSD(T)/cc-pVTZ level. The atomic spin populations, calculated from Bader AIM population analysis, are shown in Table 2 and the results of the kinetic study are given in Table 3. Finally, with the aim of assisting possible experimental work in identifying a prereactive hydrogen-bonded [H_2SO_4··· HO•] complex, designated **Cr1**, the calculated harmonic vibrational frequency, approximate assignment, and IR intensity of each normal mode for H_2SO_4, HO•, and **Cr1** are listed in Table 4S (Supporting Information).

4.1. Reactants and Products. The optimized equilibrium structure of H_2SO_4, shown in Figure 1, has C_2 symmetry with pairs of equivalents S═O (1.427 Å), S−O (1.601 Å), and H−O (0.968 Å) bond lengths, which compare well with the experimental values of 1.422, 1.574, and 0.970 Å, respectively, determined from the microwave spectrum of gaseous sulfuric acid.[60]

We found two rotational conformers for the equilibrium structure of the electronic ground-state HSO_4 radical, designated *cis*-HSO_4• and *trans*-HSO_4• (see Figure 1), which have C_s molecular symmetry and correspond to a $^2A''$ state. In both conformers the unpaired electron resides mostly on the two equivalent oxygen atoms (see Table 2). As a consequence, the

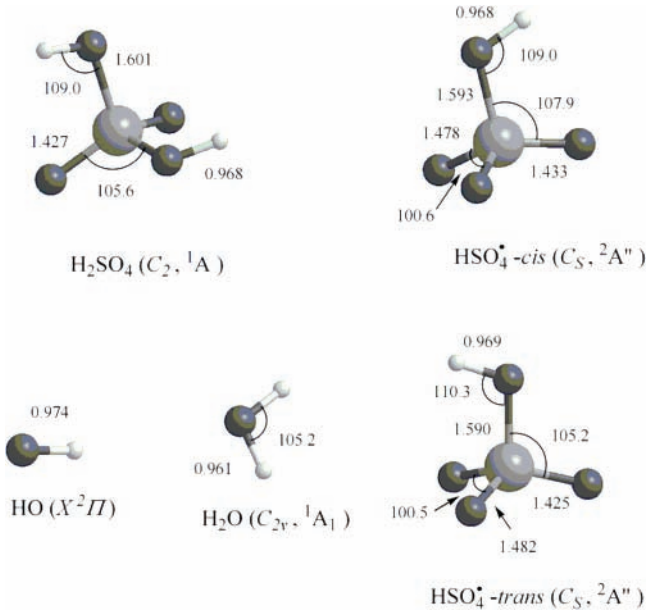

Figure 1. Selected parameters of the UB3LYP/6-311+G(2df,2p) optimized geometries of the reactants and products for hydrogen transfer between H_2SO_4 and HO•. Distances are given in Å and angles in deg.

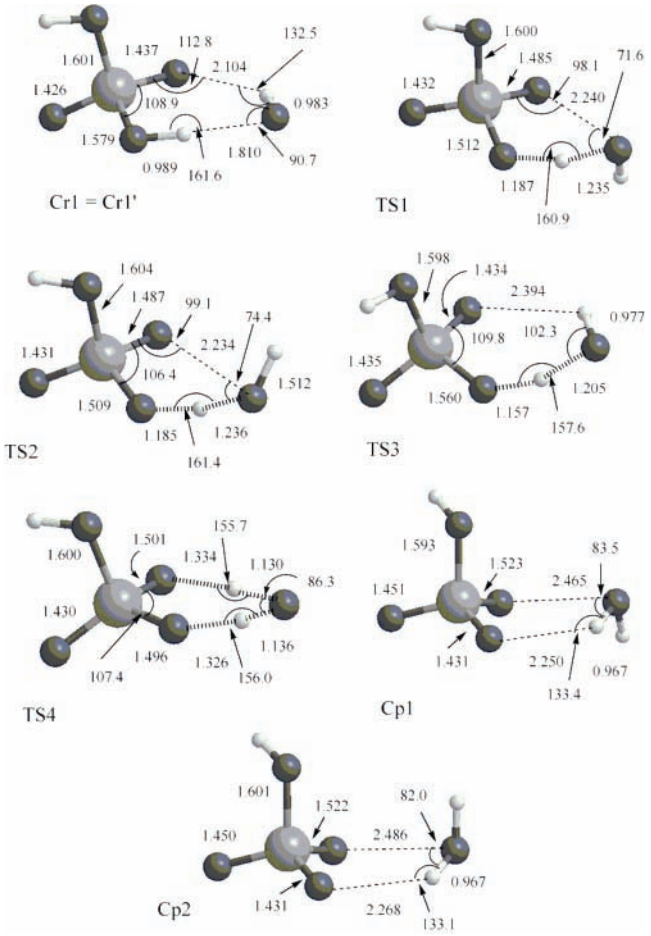

Figure 2. Selected parameters of the UB3LYP/6-311+G(2df,2p) optimized geometries of the stationary points found for hydrogen transfer between H_2SO_4 and HO•. Distances are given in Å and angles in deg.

TABLE 1: Relative Energies (kcal mol^{-1}) of the Stationary Points Involved in the Hydrogen Transfer between H_2SO_4 and HO• in the Gas Phase[a]

stationary point	ΔU	ΔE (0 K)	ΔH (298 K)	ΔG (298 K)
$H_2SO_4 + HO^•$	0.0	0.0	0.0	0.0
Cr1	−9.1 (−10.7)	−7.5 (−9.1)	−8.1 (−9.7)	−0.2 (−1.8)
TS1	2.7	2.5	1.3	10.5
Cp1	−5.8 (−8.2)	−4.0(−6.4)	−4.2 (−6.5)	2.8 (0.5)
TS2	3.0	2.7	1.6	10.5
Cp2	−5.1 (−7.5)	−3.5 (−5.9)	−3.5 (−5.9)	3.1 (0.7)
TS3	4.3	2.8	1.9	10.5
TS4	2.9	0.7	−0.7	9.0
cis-$HSO_4^•$ + H_2O	−5.2	−5.6	−5.3	−7.0
trans-$HSO_4^•$ + H_2O	−5.4	−5.6	−5.4	−6.9

[a] Calculated at the UCCSD(T)/cc-pVTZ level of theory including the BSSE correction for the **Cr1**, **Cp1**, and **Cp2** complexes. The values given in parentheses do not include the BSSE correction.

S−O bond length associated with these atoms in *cis*-$HSO_4^•$ and *trans*-$HSO_4^•$ (1.478 and 1.482 Å, respectively) turns out to be about 0.05 Å longer than in the sulfuric acid (1.427 Å), while the values of the S=O and S−O(H) bond lengths in *cis*-$HSO_4^•$, *trans*-$HSO_4^•$, and H_2SO_4 are similar in the three species.

On the basis of the relative energies ΔU listed in Table 1, *trans*-$HSO_4^•$ is found to be 0.2 kcal mol^{-1} less energetic than *cis*-$HSO_4^•$. The ΔH(298 K) calculated for *trans*-$HSO_4^•$ is 0.1 kcal mol^{-1} lower than that of *cis*-$HSO_4^•$. According to the calculated ΔH(298 K)s (see Table 1), the transfer of a single H atom from H_2SO_4 to HO• yielding *trans*-$HSO_4^•$ and H_2O (eq 4) is predicted to be exothermic by 5.4 kcal mol^{-1}. The experimental ΔH for this reaction is unknown.

4.2. Prereactive Hydrogen-Bonded Complex. As usual in many gas-phase reactions of interest in atmospheric chemistry, the reaction between H_2SO_4 and HO• begins with the formation of a prereactive hydrogen-bonded [H_2SO_4··· HO•] complex, **Cr1**, whose optimized structure (see Figure 2) was characterized as a true local minimum on the PES. As compared to the bond distances in the isolated components H_2SO_4 and HO•, the double hydrogen-bonding in **Cr1** leads to a 0.010 Å lengthening of the S4=O3 double-bond distance (see Figure 3 for atom numbering), a 0.022 Å shortening of the S4−O5 single-bond distance, a 0.021 Å lengthening of the O5−H6 bond distance, and a 0.009 Å lengthening of the O1−H2 bond distance.

A visual inspection of the occupied molecular orbitals of **Cr1** by means of the Molden program shows that the unpaired electron in the HO• moiety resides in a 2p orbital of the oxygen atom that is perpendicular to the O3−S4−O5−H6 plane and does not participate in the bond formation. The H−O bond of the HO• moiety lies on the latter plane pointing directly toward the lone pair of electrons of an oxygen atom (O3) of the H_2SO_4 moiety, whereas a hydrogen atom (H6) of the H_2SO_4 moiety is directed toward the lone pair of electrons of the oxygen atom of the HO• moiety. These electronic features, along with the short distances O1···H6 (1.810 Å) and O3···H2 (2.104 Å), suggest the formation of two hydrogen bonds between the H_2SO_4 and HO• moieties of **Cr1**, leading to a six-membered ring equilibrium structure in which the HO• acts as both a hydrogen-bond donor and a hydrogen-bond acceptor. Actually, the AIM topological analysis of the electron charge density in **Cr1** (see Table 3S, Supporting Information) reveals the presence of two bond critical points, one located between the atoms O1 and H6 ($\rho(r_b) = 0.0359$ e bohr^{-3} and $\nabla^2\rho(r_b) = 0.0984$ e bohr^{-5}) and the other located between the atoms O3 and H2 ($\rho(r_b) = 0.0187$ e bohr^{-3} and $\nabla^2\rho(r_b) = 0.0661$ e bohr^{-5}), as well as a ring critical point ($\rho(r_b) = 0.0120$ e bohr^{-3} and $\nabla^2\rho(r_b) = 0.0505$ e bohr^{-5}).

It is interesting to note that the electronic and geometric features observed for **Cr1** are very similar to those described recently for the double hydrogen-bonded complex between formic acid and hydroxyl radical.[61] However, the net atomic charges determined from the AIM population analysis predicts for the latter complex an electron charge transfer of only 0.004 e in the direction HO• → HCOOH, whereas in **Cr1** an electron charge transfer of 0.029 e in the direction HO• → H_2SO_4 is found. Therefore, the acidic moiety of complex **Cr1** shows a greater ability to bear electron charge than that of the complex between formic acid and hydroxyl radical.

At the UCCSD(T)/cc-pVTZ level of theory (see Table 1), **Cr1** lies 10.7 kcal mol^{-1} below the sum of the energies of the separated components, H_2SO_4 and HO•. Inclusion of the BSSE correction leads to a stabilization energy of **Cr1** toward decomposition into their components of 9.1 kcal mol^{-1} (see Table 1). After addition of the ZPVE correction, this binding energy is reduced to 7.5 kcal mol^{-1}, which is nearly a half of the binding energy (15.6 kcal mol^{-1}) computed at the UMP2/6-311++G(3df,3pd) level of theory for the double hydrogen-bonded complex formed by peroxy radical (HOO•) and sulfuric acid.[62]

4.3. Single Hydrogen Transfer from H_2SO_4 to HO•. According to Figure 3, after forming the prereactive hydrogen-bonded complex **Cr1**, the transfer of a single H atom from H_2SO_4 to HO• can take place through three different transition structures, designated **TS1**, **TS2**, and **TS3**. These transition

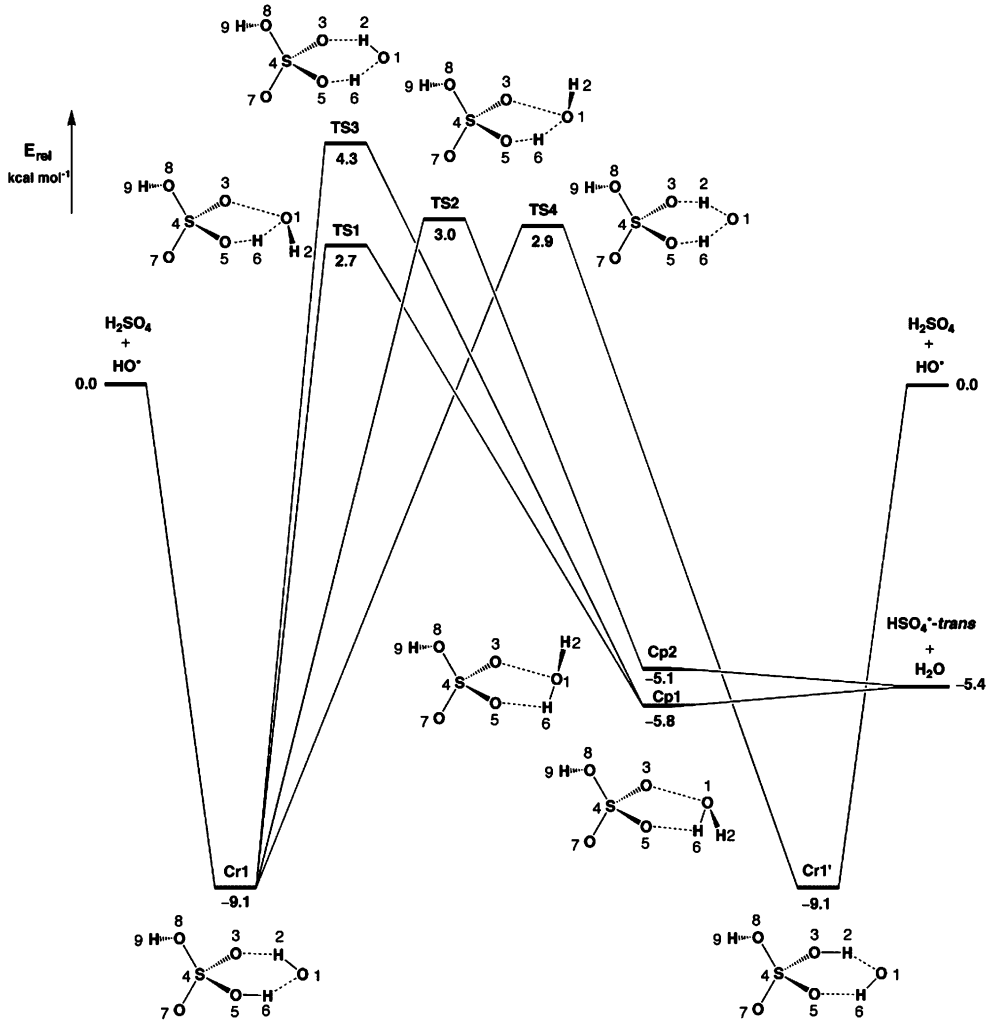

Figure 3. Schematic energy profiles along an arbitrary reaction coordinate showing the stationary points involved in the hydrogen transfer between H_2SO_4 and HO•. Relative energy values obtained from the UCCSD(T)/cc-pVTZ total energies. The BSSE-corrected total energies were used for the **Cr1**, **Cr1′**, **Cp1**, and **Cp2** complexes.

TABLE 2: Atomic Spin Populations Determined from AIM Population Analysis[a] of Stationary Points Involved in the Hydrogen Transfer between H_2SO_4 and HO• in the Gas Phase

structure	O1	H2	O3	S4	O5	H6	O7	O8	H9
Cr1	1.000	0.000	0.000	0.000	0.000	0.000	0.000	0.000	0.000
TS1	0.706	−0.008	0.278	−0.002	−0.004	−0.003	0.028	0.005	0.000
TS2	0.706	−0.008	0.278	−0.002	−0.004	−0.003	0.030	0.005	0.000
TS3	0.715	−0.007	0.007	−0.009	0.232	−0.012	0.077	0.000	0.000
TS4	0.720	−0.004	0.161	0.006	0.104	−0.002	0.011	0.005	0.000
Cp1	0.160	−0.003	0.593	−0.028	0.044	−0.002	0.238	−0.003	0.000
Cp2	0.150	−0.002	0.604	−0.028	0.051	−0.002	0.231	−0.004	0.000
cis-HSO_4•			0.473	−0.038	0.473		0.094	−0.002	0.001
trans-HSO_4•			0.469	−0.039	0.469		0.104	−0.004	0.001

[a] Using the first-order density matrix from the UB3LYP/6-311+G(2df,2p) calculations. Atom numbering refers to Figure 3.

structures differ one from the others essentially in the orientation of the HO radical with respect to the sulfuric acid (see Figure 2). While the O1−H2 bond is nearly orthogonal to O3−S4−O5−H6 plane of the sulfuric acid in **TS1** and **TS2**, it lies within this plane in **TS3**. Furthermore, **TS1** and **TS2** differ only in the orientation of the O1−H2 bond of hydroxyl radical with respect to the S4−O8 bond of sulfuric acid: **TS1** with both bonds in a *transoid* position and **TS2** in a *cisoid* position. Apart from this minor conformational difference, both transition structures show the same electronic features. In fact, a simple inspection of the occupied molecular orbitals of **TS1** and **TS2** shows that the hydroxyl radical lone pair of electrons is directed toward the hydrogen atom H6 of the sulfuric acid, whereas its unpaired electron interacts with the lone pair of electrons of the oxygen atom O3 of the sulfuric acid. In addition, Table 2 shows that the spin population in both **TS1** and **TS2** is concentrated on the oxygen atoms O1 (0.706) and O3 (0.278), whereas the spin population on the atom O5 (−0.004) is negligible. These electronic features indicate that the H atom transfer through **TS1** and **TS2** corresponds to the PCET reaction pathway depicted in Scheme 1b. The AIM analysis of the electron charge density of **TS1** and **TS2** shows the presence of a bond critical point located between the atoms O1 and O3, indicating that there is a bonding interaction between this atom pair. The small electron charge density, $\rho(r_b) = 0.0394$ (**TS1**) or $\rho(r_b) = 0.0397$ (**TS2**) e bohr^{-3}, and the positive value of the its Laplacian, $\nabla^2\rho(r_b) =$

TABLE 3: Equilibrium Constant (K_e in cm^3 molecule^{-1}; See Eq 8), Tunneling Factor (κ), Rate Constants for Elementary Reactions (k_2 in s^{-1} and k_{TS} in cm^3 molecule^{-1} s^{-1}; See Eqs 9 and 7), Overall Rate Constant ($k_{Total} = k_{TS1} + k_{TS2} + k_{TS3} + k_{TS4}$ in cm^3 molecule^{-1} s^{-1}), and Branching Ratios ($\Gamma_4 = (k_{TS1} + k_{TS2} + k_{TS3})/k_{Total}$ and $\Gamma_5 = k_{TS4}/k_{total}$ in %; See Eqs 4 and 5) Calculated for the H_2SO_4 + HO$^\bullet$ Reaction in the Gas Phase for the Temperature Range 273−320 K

	temp = 273 K	temp = 280 K	temp = 290 K	temp = 298 K	temp = 300 K	temp = 310 K	temp = 320 K
K_e	1.83×10^{-19}	1.29×10^{-19}	8.10×10^{-20}	5.71×10^{-20}	5.25×10^{-20}	3.50×10^{-20}	2.40×10^{-20}
				TS1			
κ	6.0628	5.3996	4.6549	4.1856	4.0823	3.6322	3.2715
k_2	5.70×10^3	8.66×10^3	1.53×10^4	2.36×10^4	2.63×10^4	4.37×10^4	7.08×10^4
k_{TS1}	1.04×10^{-15}	1.12×10^{-15}	1.24×10^{-15}	1.35×10^{-15}	1.38×10^{-15}	1.53×10^{-15}	1.70×10^{-15}
				TS2			
κ	5.5918	5.0064	4.3446	3.9248	3.8319	3.4261	3.0991
k_2	5.41×10^3	8.38×10^3	1.52×10^4	2.39×10^4	2.67×10^4	4.54×10^4	7.51×10^4
k_{TS2}	9.90×10^{-16}	1.08×10^{-15}	1.23×10^{-15}	1.37×10^{-15}	1.40×10^{-15}	1.59×10^{-15}	1.80×10^{-15}
				TS3			
κ	20.259	16.791	13.200	11.113	10.672	8.8376	7.4693
k_2	1.85×10^4	2.68×10^4	4.48×10^4	6.66×10^4	7.33×10^4	1.17×10^5	1.84×10^5
k_{TS3}	3.38×10^{-15}	3.46×10^{-15}	3.63×10^{-15}	3.80×10^{-15}	3.85×10^{-15}	4.10×10^{-15}	4.42×10^{-15}
				TS4			
κ	2.6079	2.4394	2.2376	2.1019	2.0710	1.9316	1.8136
k_2	4.17×10^4	6.09×10^4	1.01×10^5	1.49×10^5	1.63×10^5	2.56×10^5	3.91×10^5
k_{TS4}	7.64×10^{-15}	7.86×10^{-15}	8.21×10^{-15}	8.51×10^{-15}	8.58×10^{-15}	8.98×10^{-15}	9.39×10^{-15}
k_{total}	1.30×10^{-14}	1.35×10^{-14}	1.43×10^{-14}	1.50×10^{-14}	1.52×10^{-14}	1.62×10^{-14}	1.73×10^{-14}
Γ_4	41.5	41.9	42.6	43.4	43.6	44.6	45.8
Γ_5	58.5	58.1	57.4	56.6	56.4	55.4	54.2

0.1684 (**TS1**) or $\nabla^2\rho(r_b) = 0.1683$ (**TS2**) e bohr^{-5}, calculated for this bond critical point (see Table 3S, Supporting Information) suggest that O1 and O3 are weakly bonded by a noncovalent interaction. As in the case of the transition structure computed for the transference of the acidic H atom of formic acid to the hydroxyl radical through the PCTE mechanism, this noncovalent interaction enables the transfer of a single electron from the sulfuric acid to the hydroxyl radical.[51,52]

With regard to transition state **TS3**, it is worth noting that the hydroxyl radical moiety is oriented in such a way that its unpaired electron interacts with hydrogen atom H6 of the sulfuric acid moiety, giving a three-center three-electron bond (O1···H6···O5). In fact, Table 2 shows that the spin population in **TS3** is concentrated on the oxygen atoms O1 (0.715) and O5 (0.232) between which the hydrogen atom is being transferred with a small negative value (−0.012) on the hydrogen atom. These findings suggest that the H atom transfer through **TS3** takes place by the HAT reaction pathway depicted in Scheme 1a. At the same time, the somewhat short distance (2.394 Å) between atoms O3 and H2 in **TS3** suggests a weak hydrogen-bonding interaction between these atoms. Actually, the AIM analysis of the electron charge density in **TS3** (see Table 3S, Supporting Information) reveals the presence of a bond critical point located between the atoms O3 and H2 ($\rho(r_b) = 0.0115$ e bohr^{-3} and $\nabla^2\rho(r_b) = 0.0433$ e bohr^{-5}). Although this weak hydrogen-bonding interaction is expected to lower somewhat the energy of **TS3**, the ΔU data listed in Table 1 show that the relative energies of the PCET transition states **TS1** (2.7 kcal mol^{-1}) and **TS2** (3.0 kcal mol^{-1}) are lower than that of the HAT transition state **TS3** (4.3 kcal mol^{-1}). On the basis of the calculated atomic spin populations, the lower energy of the PCET transition structures as compared to that of the HAT transition structures in the hydrogen transfer from the OH group to oxygen-centered radicals have been ascribed recently to the fact that the triplet repulsion between the unpaired electrons located at the oxygen atoms undergoing hydrogen exchange must be lower in the transition structures for a PCET pathway than in the transition structure for a HAT pathway.[51] However, Table 1 shows that after addition of the ZPVE and thermal correction to enthalpy, the energy differences among **TS1**, **TS2**, and **TS3** is reduced to a few tenths of kilocalorie per mole. Furthermore, inclusion of the entropy changes leads to the same value (10.5 kcal mol^{-1}) of $\Delta G(298\ K)$ for the three transition structures. Therefore, the simple ΔU energy differences are not meaningful and cannot be used to discriminate one mechanism (PCET) from the other (HAT). At any rate, the single H atom transfer from H_2SO_4 to HO$^\bullet$ (eq 4) involves a 298 K small activation enthalpy ranging from 1.3 to 1.9 kcal mol^{-1}. It can be concluded that this reaction may play a significant role in the atmospheric degradation of gaseous H_2SO_4.

The IRC calculations showed that both **TS1** and **TS3** go forward to the hydrogen-bonded complex between the reaction products *trans*-HSO$_4^\bullet$ and H_2O, designated **Cp1**, whereas **TS2** goes forward to another hydrogen-bonded complex between these species, designated **Cp2**. The optimized geometries of these complexes (see Figure 2) were characterized as true local minima on the PES. **Cp1** and **Cp2** differ one from the other in the conformation: **Cp1** with the O1−H2 bond in a *transoid* position toward the S4−O8 bond, and **Cp2** with the O1−H2 bond in a *cisoid* position. The AIM analysis of the electron charge density of **Cp1** and **Cp2** (see Table 3S, Supporting Information) revealed the presence of two bond critical points, one located between the atoms O5 and H6, indicating a weak hydrogen bond between these atoms, and the other located between the atoms O3 and O1, suggesting that these atoms remain weakly bonded by the same noncovalent interaction noted above for **TS1** and **TS2**. The latter interaction is consistent with the fact that the spin population on the oxygen atom O1 of **Cp1** and **Cp2** (0.160 and 0.150, respectively) is still significant. The combination of the O5···H6 hydrogen bond and that noncovalent interaction between atoms O3 and O1 leads to the formation of a five-membered ring equilibrium structure for complexes **Cp1** and **Cp2**. In keeping with this structural feature, the AIM analysis of the electron charge density of **Cp1** and **Cp2** indicated the presence of a ring critical point (see Table 3S, Supporting Information). At the UCCSD(T)/cc-pVTZ level of theory (see Table 1), **Cp1** and **Cp2** lie 2.7 and 2.1 kcal mol^{-1}, respectively, below the sum of the energies of the separated reaction products, *trans*-HSO$_4^\bullet$ and H_2O. However, inclusion of the corrections for the BSSE reduces the binding energy of **Cp1** to only 0.4 kcal mol^{-1} and places the energy of **Cp2** at

0.3 kcal mol^{-1} above that of the isolated components *trans*-$HSO_4^{\bullet}$ and H_2O. Furthermore, after addition of the ZPVE corrections, the energies of both **Cp1** and **Cp2** are predicted to be 1.6 and 2.1 kcal mol^{-1}, respectively, higher than the sum of the energies of the separated reaction products. These results lessen the relevance of these complexes between the reaction products.

4.4. Double Hydrogen Transfer between H_2SO_4 and HO$^{\bullet}$. As shown in Figure 3, after forming the prereactive hydrogen-bonded complex **Cr1**, the concerted transfer of two hydrogen atoms between H_2SO_4 and HO$^{\bullet}$ takes place through the transition structure designated **TS4**, whose optimized geometry is displayed in Figure 2. It is worth noting that **TS4** connects the equilibrium structures of the prereactive complex **Cr1** with an equivalent equilibrium structure of the same complex, designated **Cr1′**. Interestingly, though the double hydrogen-exchange process **Cr1** → **Cr1′** is a degenerate reaction, the optimized geometry of **TS4** turns out to be unsymmetrical (C_1). In particular, we note that the dihedral angle O7−S4−O8−H9 of **TS4** is calculated to be 24.2°. At this point, it is also worth noting that in the **Cr1** complex such a dihedral angle is found to be 29.0°. These findings are a consequence of the C_2 symmetry found for the equilibrium geometry of H_2SO_4, which shows a dihedral angle O7−S4−O8−H9 of 26.8°.

From the electronic structure point of view, the most remarkable feature of **TS4** is that the unpaired electron resides in a molecular orbital perpendicular to the O3−S4−O5 plane, while the molecular orbitals describing the bonds involved in the double hydrogen-exchange between the H_2SO_4 and HO$^{\bullet}$ moieties lie on this plane. Therefore, the unpaired electron does not participate in the double hydrogen-exchange process. As shown in Table 2, most of the spin population (0.720) resides on the oxygen atom of the HO$^{\bullet}$ moiety of **TS4**, though the spin population on the oxygen atoms O3 (0.161) and O5 (0.104) of the H_2SO_4 moiety is significant. These results suggest that there is a delocalization of the hydroxyl radical unpaired electron to the oxygen atoms O3 and O5 in **TS4**, which arises from a weak overlap among the 2p orbitals of the O1, O3 and O5 atoms that are perpendicular to the O3−S4−O5 plane. At the same time, a visual inspection of the occupied molecular orbitals reveals that the lone pair of electrons on the oxygen atom of the hydroxyl radical moiety interacts with the H6 atom of the sulfuric acid moiety, while the hydrogen atom of the hydroxyl radical moiety interacts with the lone pair of electrons on the O3 atom of the sulfuric acid. These hydrogen-bonding-like interactions indicate that the double hydrogen transfer between sulfuric acid and hydroxyl radical through **TS4** takes place by the DPT reaction pathway depicted in Scheme 1c.

The ΔU data listed in Table 1 show that **TS4** lies 2.9 kcal mol^{-1} above the sum of the energies of the separated reactants, H_2SO_4 and HO$^{\bullet}$, and only 0.2 kcal mol^{-1} above the lowest energy transition structure **TS1**. However, the ΔH(298 K) calculated for **TS4** is 0.7 kcal mol^{-1} lower than that of the separated reactants. Furthermore, according to the calculated $\Delta G^{\ddagger}$(298 K), **TS4** is the transition structure for the hydrogen transfer between H_2SO_4 and HO$^{\bullet}$ involving the lowest free energy of activation at 298 K ($\Delta G^{\ddagger}$(298 K)) (i.e., 9.0 kcal mol^{-1}). Therefore, the degenerate double hydrogen-exchange reaction eq 5 turns out to be the most favorable hydrogen transfer reaction between H_2SO_4 and HO$^{\bullet}$ in the gas phase. These findings are in clear contrast with the results obtained for the hydrogen transfer between formic acid and hydroxyl radical predicting for the double hydrogen-exchange a $\Delta G^{\ddagger}$(298 K) of 15.9 kcal mol^{-1}, which is 3.4 kcal mol^{-1} higher than the $\Delta G^{\ddagger}$(298 K) for the acidic hydrogen transfer from the formic acid to the hydroxyl radical through a PCET mechanism.[52]

Although the degenerate double hydrogen-exchange reaction eq 5 is a silent reaction, namely where the reactants and the products are the same species, this reaction might be experimentally observed if one of both reactants was conveniently deuterated. For instance, the reaction between H_2SO_4 and DO$^{\bullet}$ should lead to deuterium scrambling in the sulfuric acid, so the formation of products such as $HDSO_4$ and D_2SO_4 could be observed. However, in the presence of water there will be also fast deuterium scrambling by acid−base reactions between sulfuric acid and water, and therefore, the degenerate double hydrogen exchange cannot be validated.

4.5. Kinetics. As noted above, the double hydrogen-exchange reaction eq 5 is predicted to be the most favorable hydrogen transfer reaction between H_2SO_4 and HO$^{\bullet}$ in the gas phase. However, the single hydrogen transfer from H_2SO_4 and HO$^{\bullet}$ (eq 4) through any of the transition structures **TS1**, **TS2**, and **TS3** involves a $\Delta G^{\ddagger}$(298 K) of 10.5 kcal mol^{-1}, which is only 1.5 kcal mol^{-1} higher than the $\Delta G^{\ddagger}$(298 K) of 9.0 kcal mol^{-1} calculated for the double-hydrogen exchange reaction. With the aim for investigating whether the single hydrogen transfer from H_2SO_4 and HO$^{\bullet}$ could play a significant role in the atmospheric degradation of gaseous H_2SO_4, we have employed the conventional transition state theory to estimate a possible competition between reactions eqs 4 and 5 and to evaluate the rate constant for the overall H_2SO_4 plus HO$^{\bullet}$ reaction.

It has been shown in the previous sections that in both reactions eqs 4 and 5 a prereactive hydrogen-bonded complex **Cr1** is formed before either the single hydrogen or the double hydrogen transfers occur. Therefore, each reaction is a two-step reaction as described by eq 6, where the complex is in equilibrium with the reactants

$$H_2SO_4 + HO^{\bullet} \underset{k_{-1}}{\overset{k_1}{\rightleftharpoons}} \text{complex} \xrightarrow{k_2} \text{products} \qquad (6)$$

and the rate constant for each process is given by eq 7.

$$k_1 = \frac{k_1}{k_{-1}} k_2 = K_{eq} k_2 \qquad (7)$$

The equilibrium constant K_{eq} in the first step and the rate constant k_2 of the second step of eq 6 are given by eqs 8 and 9, respectively,

$$K_{eq} = \sigma \frac{Q_{Complex}}{Q_{H_2SO_4} Q_{OH}} e^{-(E_C - E_R)/RT} \qquad (8)$$

$$k_2 = \kappa\sigma \frac{k_b T}{h} \frac{Q_{TS}}{Q_{Complex}} e^{-(E_{TS} - E_C)/RT} \qquad (9)$$

where the various Q denote the partition functions of the reactants H_2SO_4 and HO$^{\bullet}$, the prereactive hydrogen-bonded complex, and the transition state; E_R, E_C, and E_{TS} are the total electronic energies of the reactants, hydrogen-bonded complex, and transition state, respectively; k_b and h are the Boltzmann and Planck constants, respectively, κ is the tunneling factor, σ is the symmetry number, and T is the absolute temperature. The rate constants were calculated in the range of temperatures between 273 and 320 K.

The results displayed in Table 3 predict an overall rate constant, k_{total}, of 1.50×10^{-14} cm^3 molecule^{-1} s^{-1} at 298 K for the H_2SO_4 + HO$^{\bullet}$ reaction and a small temperature

dependence (a factor of 1.33) in the range of temperatures considered. The experimental rate constant of this reaction is unknown. However, it is interesting to note that for the HCOOH + HO• reaction a rate constant of 6.24×10^{-13} cm^3 molecule^{-1} s^{-1} at 298 K was predicted by using theoretical calculations similar to those performed here.[52] The latter rate constant is about a factor of 42 higher than our predicted value for the H_2SO_4 + HO• reaction. With regard to the elementary reactions contributing to the overall rate constant for the H_2SO_4 + HO• reaction, Table 3 shows that, as expected from the free energy results given in Table 1, the degenerate double hydrogen-exchange (eq 5) through **TS4** is the dominant reaction. However, the single hydrogen transfer through **TS1**, **TS2**, and **TS3**, giving HSO_4• and H_2O (eq 4), contributes to the overall rate constant with a percentage changing from 41.5 to 45.8% for the range of temperatures considered. Therefore, it is concluded that reaction eq 4 might play a significant role in the atmospheric degradation of gaseous H_2SO_4.

5. Summary and Conclusions

In this paper, we have investigated by means of DFT and quantum-mechanical electronic-structure calculations, as well as classical transition state theory computations, the hydrogen transfer between H_2SO_4 and HO• in the gas phase, in an attempt to asses the potential role of this reaction in the atmospheric degradation of gaseous H_2SO_4. From the analysis of the results the following main points emerge:

(1) The first step of the H_2SO_4 + HO• reaction is the barrierless formation of a prereactive hydrogen-bonded complex lying 8.1 kcal mol^{-1} below the sum of the (298 K) enthalpies of the reactants. After forming the prereactive complex, a single hydrogen transfer from H_2SO_4 to HO•, yielding HSO_4• and H_2O, and a double hydrogen-exchange between H_2SO_4 and HO•, affording products identical to the reactants, can occur.

(2) The single hydrogen transfer from H_2SO_4 to HO• can take place through three different transition structures. The two lowest energy transition structures (**TS1** and **TS2**) correspond to a proton-coupled electron transfer (PCET) mechanism, whereas the higher energy transition structure (**TS3**) corresponds to a hydrogen atom transfer (HAT). Inclusion of the ZPVE, the thermal correction to enthalpy, and the entropy change, leads to a $\Delta G^{\ddagger}$(298 K) of 10.5 kcal mol^{-1} for the three reaction pathways associated with **TS1**, **TS2**, and **TS3**.

(3) The degenerate double hydrogen-exchange between H_2SO_4 and HO• takes place through a transition structure (**TS4**) involving a double proton transfer (DPT) mechanism with a $\Delta G^{\ddagger}$(298 K) of 9.0 kcal mol^{-1}. The reaction H_2SO_4 + HO•, therefore, is predicted to occur preferably via double hydrogen-exchange between H_2SO_4 and HO•, rather than by single hydrogen transfer from H_2SO_4 to HO•.

(4) A rate constant of 1.50×10^{-14} cm^3 molecule^{-1} s^{-1} at 298 K is predicted for the overall H_2SO_4 + HO• reaction. Although the degenerate double hydrogen-exchange through **TS4** is the dominant reaction, the single hydrogen transfer through **TS1**, **TS2**, and **TS3**, contributes to the overall rate constant at 298 K with a 43.4%. Therefore, the H_2SO_4 + HO• reaction leading to the formation of HSO_4• and H_2O might be expected to contribute significantly to the fate of gaseous sulfuric acid in the atmosphere.

Acknowledgment. This research was supported by the Spanish DGICYT (Grants BQU2002-0485-C02-01 and BQU2002-0485-C02-02) and the Catalonian DURSI (Grant 2001SGR00048). The larger calculations described in this work were performed at the Centre de Supercomputació de Catalunya (CESCA).

Supporting Information Available: Tables 1S−4S, summarizing the Cartesian coordinates of all structures reported in this paper, total electronic energies, zero-point vibrational energies, enthalpies, Gibbs free energies, absolute entropies, topological properties of the electron charge density, and harmonic vibrational frequencies and IR intensity of each normal mode for H_2SO_4, HO•, and **Cr1**, and Figure 1S, showing the geometries of the transition structures optimized at the UQCISD/6-31+G(d,p) level). This material is available free of charge via the Internet at http://pubs.acs.org.

References and Notes

(1) Calvert, J. G.; Lazrus, A.; Kok, G. L.; Heikes, B. G.; Walega, J. G.; Lind, H.; Cantrell, C. A. *Nature* **1985**, *317*, 27.
(2) Wayne, R. P. *Chemistry of Atmospheres*, 3rd ed., Oxford University Press: Oxford, U.K., 2000.
(3) Jacob, D. J. *Introduction to Atmospheric Chemistry*, Princeton University Press: Princeton, NJ, 1999.
(4) Charlson, R. J.; Langner, J.; Rodhe, H.; Leovy, C. B.; Warren, S. G. *Tellus* **1993**, *43B*, 152.
(5) Kiehl, J. T.; Briegleb, B. P. *Science* **1993**, *260*, 311.
(6) Eisele, F. L.; McMurry, P. H. *Philos. Trans. R. Soc. London, B* **1997**, *352*, 191.
(7) Venkataraman, C.; Mehra, A.; Mhaskar, P. *Tellus* **2001**, *53B*, 260.
(8) Pham, M.; Mueller, J. F.; Brasseur, G. P.; Grainer, C.; Mégie, G. *J. Geophys. Res.* **1995**, *100*, 26061.
(9) Chin, M.; Jacob, D. J.; Gardner, G. M.; Foreman-Fowler, M. S.; Spiro, P. A. *J. Geophys. Res.* **1996**, *101*, 18667.
(10) Li, W.-K.; McKee, M. L. *J. Phys. Chem. A* **1997**, *101*, 9778.
(11) Blitz, M. A.; Hughes, K. J.; Pilling, M. J. *J. Phys. Chem. A* **2003**, *107*, 1971.
(12) Somnitz, H. *Phys. Chem. Chem. Phys.* **2004**, *6*, 3844.
(13) Majumdar, D.; Kim, G.-S.; Kim, J.; Oh, K. S.; Lee, J. Y.; Kima, K. S. *J. Chem. Phys.* **2000**, *112*, 723.
(14) Aaltonen, E. T.; Francisco, J. S. *J. Phys. Chem. A* **2003**, *107*, 1216.
(15) Morokuma, K.; Muguruma, C. *J. Am. Chem. Soc.* **1994**, *116*, 10316.
(16) Loerting, T.; Liedl, K. R. *Proc. Natl. Acad. Sci.* **2000**, *96*, 8874.
(17) Loerting, T.; Liedl, K. R. *J. Phys. Chem. A* **2001**, *105*, 5135.
(18) Jefferson, A.; Tanner, D. J.; Eisele, F. L.; Davis, D. D.; Chen, G.; Crawford, J.; Huey, J. W.; Torres, A. L.; Berresheim, H. *J. Geophys. Res.* **1995**, *103 D1*, 1647.
(19) Bardouki, H.; Berresheim, H.; Vrekoussis, M.; Sciare, J.; Kouvaraskis, G.; Oikonomou, K.; Schneider, J.; Mihalopoulos, N. *Atmos. Chem. Phys.* **2003**, *3*, 1871.
(20) Legrand, M.; Angelis, M. D. *J. Geophys. Res.* **1995**, *100*, 1445.
(21) Grosjean, D. *Environ. Sci. Technol.* **1989**, *23*, 1506.
(22) Puxbaum, H.; Rosenberg, C.; Gregori, M.; Lanzerstorfer, C.; Ober, E.; Winiwarter, W. *Atmos. Environ.* **1988**, *22*, 1841.
(23) Sanhueza, E.; Santana, M.; Hermoso, M. *Atmos. Environ.* **1992**, *26a*, 1421.
(24) Granby, K.; Christensen, C. S.; Lohse, C. *Atmos. Environ.* **1997**, *31*, 1403.
(25) Kesselmeier, J. *J. Atmos. Chem.* **2001**, *39*, 219.
(26) Becke, A. D. *J. Chem. Phys.* **1993**, *98*, 5648.
(27) Lee, C.; Yang, W.; Parr, R. G. *Phys. Rev. B* **1988**, *37*, 785.
(28) Stevens, P. J.; Devlin, F. J.; Chablowski, C. F.; Frisch, M. J. *J. Phys. Chem.* **1994**, *98*, 11623.
(29) Frisch, M. J.; Pople, J. A.; Binkley, J. S. *J. Chem. Phys.* **1984**, *80*, 3265.
(30) Hehre, W. J.; Radom, L.; Schleyer, P. v. R.; Pople, J. A. *Ab Initio Molecular Orbital Theory*; John Wiley: New York, 1986; pp 86−87.
(31) Fukui, K. *Acc. Chem. Res.* **1981**, *14*, 363.
(32) Ishida, K.; Morokuma, K.; Kormornicki, A. *J. Chem. Phys.* **1977**, *66*, 2153.
(33) Gonzalez, C.; Schlegel, H. B. *J. Chem. Phys.* **1989**, *90*, 2154.
(34) Gonzalez, C.; Schlegel, H. B. *J. Phys. Chem.* **1990**, *94*, 5523.
(35) Pople, J. A.; Head-Gordon, M.; Raghavachari, K. *J. Chem. Phys.* **1987**, *87*, 5968.
(36) Basch, H.; Hoz, S. *J. Phys. Chem. A* **1997**, *101*, 4416−4431.
(37) For a review, see: Bartlett, R. J. *J. Phys. Chem.* **1989**, *93*, 1967.
(38) Raghavachari, K.; Trucks, G. W.; Pople, J. A.; Head-Gordon, M. *Chem. Phys. Lett.* **1989**, *157*, 479.
(39) Dunning, T. H. *J. Chem. Phys.* **1989**, *90*, 1007.

(40) Kendall, R. A.; Dunning, T. H.; Harrison, R. J. *J. Chem. Phys.* **1992**, *96*, 6796.

(41) Boys, S. F.; Bernardi, F. *Mol. Phys.* **1970**, *19*, 553.

(42) Bader, R. F. W. *Atoms in Molecules. A Quantum Theory*; Clarendon Press: Oxford, U.K., 1990.

(43) Truong, T. N.; Truhlar, D. G. *J. Chem. Phys.* **1990**, *93*, 1761.

(44) Frisch, M. J.; Trucks, G. W.; Schlegel, H. B.; Scuseria, M. A.; Robb, M. A.; Cheeseman, J. R.; Zakrzewski, V. G.; Montgomery, J. A.; Stratmann, R. E.; Burant, J. C.; Dapprich, S.; Milliam, J. M.; Daniels, A. D.; Kudin, K. N.; Strain, M. C.; Farkas, O.; Tomasi, J.; Barone, V.; Cossi, M.; Cammi, R.; Mennucci, B.; Pomelli, C.; Adamo, C.; Clifford, S.; Ochterski, J.; Petersson, G. A.; Ayala, P. Y.; Cui, Q.; Morokuma, K.; Malick, D. K.; Rabuck, A. D.; Raghavachari, K.; Foresman, J. B.; Cioslowski, J.; Ortiz, J. V.; Stefanow, B. B.; Liu, G.; Liashenko, A.; Piskorz, P.; Komaromi, A.; Gomperts, R.; Martin, R. L.; Fox, D. J.; Keith, T.; Al-Laham, M. A.; Peng, C. Y.; Nanayakkara, A.; Gonzalez, C.; Challacombe, M.; Gill, P. M. W.; Johnson, B. G.; Chen, W.; Wong, M. W.; Andres, J. L.; Head-Gordon, M.; Replogle, E. S.; Pople, J. A. *GAUSSIAN 98 (Revision A.11)*; Gaussian, Inc.: Pittsburgh, PA, 1998.

(45) Shaftenaar, G.; Noordik, J. H. *J. Comput.-Aided Mol. Design* **2000**, *14*, 123.

(46) Mota, F. Universitat de Barcelona.

(47) Biegler-König, F. W.; Bader, R. F. W.; Tang, T.-H. *J. Comput. Chem.* **1982**, *3*, 317.

(48) Bader, R. F. W.; Tang, T.-H.; Tal, Y.; Biegler-König, F. W. *J. Am. Chem. Soc.* **1982**, *104*, 946.

(49) Duncan, W. T.; Troung, T. N. http://therate.hec.utah.edu, downloaded September 2000.

(50) Mayer, J. M.; Hrovat, D. A.; Thomas, J. L.; Borden, W. T. *J. Am. Chem. Soc.* **2002**, *124*, 11142.

(51) Olivella, S.; Anglada, J. M.; Solé, A.; Bofill, J. M. *Chem.—Eur. J.* **2004**, *10*, 3404.

(52) Anglada, J. M. *J. Am. Chem. Soc.* **2004**, *126*, 9809.

(53) For a recent review on PCET reactions see: Mayer, J. M. *Annu. Rev. Phys. Chem.* **2004**, *55*, 363 390.

(54) Zavitsas, A. A.; Chatgilialoglu, C. *J. Am. Chem. Soc.* **1995**, *117*, 10645.

(55) Zavitsas, A. A. *J. Chem. Soc., Perkin Trans. 2* **1996**, 391.

(56) Zavitsas, A. A. *J. Am. Chem. Soc.* **1998**, *120*, 6578.

(57) Foti, M.; Ingold, K. U.; Lusztyk, J. *J. Am. Chem. Soc.* **1994**, *116*, 9440.

(58) Song, L.; Wu, W.; Hiberty, P. C.; Danovich, D.; Shaik, S. *Chem.—Eur. J.* **2003**, *9*, 4540.

(59) The Cartesian coordinates of all structures optimized at the UB3LYP/6-311+G(2df,2p) level are given in Table 1S (Supporting Information). The most relevant geometrical parameters of the transition structures optimized at the UQCISD/6-31+G(d,p) level are shown in Figure 1S (Supporting Information).

(60) Kuczkowski, R. L.; Suenram, R. D.; Loras, F. J. *J. Am. Chem. Soc.* **1981**, *103*, 2561.

(61) Torrent-Sucarrat, M.; Anglada, J. M. *ChemPhysChem* **2004**, *5*, 183.

(62) Miller, C. E.; Francisco, J. S. *J. Am. Chem. Soc.* **2001**, *123*, 10387—10388.